applied sciences

MDPI

Article

Fluorescence Lifetime Phasor Analysis and Raman Spectroscopy of Pigmented Organic Binders and Coatings Used in Artworks

Alice Dal Fovo [1,*], Sara Mattana [1], Antonina Chaban [1], Diego Quintero Balbas [1], João Luis Lagarto [1,2], Jana Striova [1], Riccardo Cicchi [1,2] and Raffaella Fontana [1]

[1] National Research Council—National Institute of Optics (CNR-INO), Largo E. Fermi 6, 50125 Florence, Italy; sara.mattana@ino.cnr.it (S.M.); antonina.chaban@ino.cnr.it (A.C.); diegoivan.quinterobalbas@ino.cnr.it (D.Q.B.); joao.lagarto@research.fchampalimaud.org (J.L.L.); jana.striova@ino.cnr.it (J.S.); riccardo.cicchi@ino.cnr.it (R.C.); raffaella.fontana@ino.cnr.it (R.F.)

[2] European Laboratory for Non-linear Spectroscopy (LENS), Via Nello Carrara 1, 50019 Sesto Fiorentino, Italy

* Correspondence: alice.dalfovo@ino.cnr.it

Abstract: Fluorescence analysis of materials used as binders and coatings in artworks is often hampered by numerous factors, leading to uncertainties in data interpretation. Fluorescence lifetime (FL) measurements enable improvement of the specificity with respect to steady-state measurements by resolving the decay dynamics of the fluorophore emissions. In this work, layers of natural resin, oil, and wax—in pure form, pigmented, in mixtures, and spread on different substrates—were analyzed using a compact, portable, fiber-based FL instrument. FL data were processed via the phasor method and integrated with Raman spectroscopy to obtain complementary chemical information on the different substances. It was observed that the τ-phase of the mixtures is affected by both the pigments and the dispersing medium, and that the presence of the metal substrate contributes to changes in the FL of mixtures. The results obtained with our portable FL system combined with Raman spectroscopy pave the way for a systematic study of a larger number of materials for future in situ applications on works of art.

Keywords: fluorescence lifetime; Raman spectroscopy; phasor analysis; organic binders; fluorescent pigments

Citation: Dal Fovo, A.; Mattana, S.; Chaban, A.; Quintero Balbas, D.; Lagarto, J.L.; Striova, J.; Cicchi, R.; Fontana, R. Fluorescence Lifetime Phasor Analysis and Raman Spectroscopy of Pigmented Organic Binders and Coatings Used in Artworks. *Appl. Sci.* **2022**, *12*, 179. https://doi.org/10.3390/app12010179

Academic Editor: Herbert Schneckenburger

Received: 30 November 2021
Accepted: 23 December 2021
Published: 24 December 2021

1. Introduction

Fluorescence is a photoinduced luminescence (PL) emission from a molecule's singlet excited state. The intensity, polarization, spectral features, and decay time (typically from 10^{-9} to 10^{-7} s [1]) of the fluorescence emission can be related to the emitting molecular species.

UV-excited fluorescence has long been applied as a simple photographic technique for the non-invasive qualitative examination of artworks to assess the presence of intrinsically luminescent materials typically employed in cultural heritage (CH) [2–5]. By exposing the object's surface to the light of a low-pressure mercury lamp, the distribution of coatings not perceivable to the naked eye—such as protective varnishes and restoration materials—can be revealed by the color difference of their fluorescence emissions [6]. In recent years, with the introduction of spectrally resolved laser-induced fluorescence (LIF) analysis [7–9], a broader number of luminescent organic and inorganic compounds have been investigated, including proteins, oils, waxes, resins, and pigments [8,10–12].

Despite the widespread use of PL techniques, it is well recognized that the identification of fluorescent species based on their spectra alone can prove complex and misleading, confirming that the combination of complementary analytical techniques is often the best choice when using a non-invasive approach [13]. Difficulties in data interpretation are mainly due to intrinsic similarities in the emission spectra of different fluorophores, and to

the fact that the detected signal is often generated by multiple species. Subtle spectral differences can be caused by the influence of the molecular environment, as well as by chemical modifications of the bulk material and competing optical phenomena, such as (self-) absorption and/or scattering [8,14,15]. Furthermore, the presence of non-fluorescent pigments dispersed in protein- and oil-based organic binders can strongly affect the emissions of the latter [14,16,17], sometimes obliterating them with optical absorption or quenching effects and, thus, producing false-negative results [12]. These factors may significantly hamper the application of fluorescence spectroscopy in CH studies, especially when the goal is the identification and mapping of coating materials. However, it has been demonstrated that the interpretation of the signal emitted by complex organic molecules—such as the fatty acids and proteins composing most binding and protective media [18,19]—can be greatly facilitated by the analysis of the dynamic nature of their fluorescence emissions. Specifically, time-resolved photoluminescence (TRPL) spectroscopy and fluorescence lifetime (FL) spectroscopy and imaging are enable to enhance the specificity of fluorescence measurements by resolving the emission decay dynamics of fluorophores characterized by overlapping emission spectra but different fluorescence lifetimes. For example, FL imaging is particularly well suited for spatial mapping of compositional heterogeneities over an examined area, taking advantage of the fact that the emission lifetime is insensitive to changes in the concentration of the emitting material, as well as being independent of the fluorescence intensity [20]. Moreover, the effectiveness of the integration of time-resolved fluorescence with complementary analytical methods—such as Raman spectroscopy and X-ray fluorescence—has been proven by several applications on paintings [6,21,22], sculptures, and plastic-based objects [23], allowing in some cases for the detection of even the presence of superimposed organic materials [18]. The advantages offered by a synergic application of Raman and PL spectroscopy are well demonstrated by the recent development of hybrid setups based on a single pulsed laser source [22,24,25]. Studies based on time-resolved fluorescence techniques have made it possible to characterize the emission lifetimes of many art materials, such as those of inorganic fluorescent pigments—i.e., cadmium-based pigments, zinc white, titanium white, chrome yellow, ultramarine and cinnabar—which are in the order of picoseconds. A much longer luminescence decay time (107 μs) is characteristic of Egyptian blue—the synthetic blue pigment based on cuprorivaite [26]. Other natural organic pigments—such as lakes or diazo pigments—and synthetic organic dyes (including phthalocyanines and anthraquinones) [27] show band-gap emission in the order of picoseconds or nanoseconds. Similar decay kinetics are characteristic of the long-chain organic molecules that make up resins, waxes, binders, and glues, which are highly influenced by several factors, including pH, temperature, and molecular flexibility [15].

To conclude, in order to improve the versatility of PL techniques in the CH, field it is essentially necessary to consider two aspects: First, the complexity of the chemical nature of art materials, as well as the variety of factors affecting their fluorescence emissions, require the definition of new approaches for the correct interpretation of time-resolved fluorescence analysis. Second, the fragility of most CH objects requires that non-invasive investigations are applied in situ in order to avoid unnecessary displacement of artworks, which could compromise their material integrity.

In this preliminary study, we propose the use of a novel handheld fiber-based FL system [28,29] to discriminate luminescent organic and inorganic compounds based on their different emission lifetimes. Purposely prepared layers of natural resin, oil and wax—in pure form, pigmented, in mixtures, and spread on different substrates—were selected as a representative set of binders and material coatings commonly found in the form of patina on historical paintings and metal-based sculptures [30]. Fluorescence measurements were time-resolved by means of time-correlated single-photon counting (TCSPC), given its higher temporal resolution, sensitivity, and dynamic range compared to other time-resolved methods. FL data were processed via the phasor method and integrated with micro-Raman spectroscopy to obtain complementary chemical information on the compounds. This is

the first time that the proposed system, originally developed for biological and biomedical applications, has been used for the analysis of artistic materials.

2. Materials and Methods

2.1. Samples

Some of the materials typically used as binders and coatings in artworks—specifically, linseed oil (LO), mastic (M) (a triterpenoid resin) [10], and beeswax (BW)—were selected for the combined FL–Raman spectroscopy analysis. The materials were examined either in pure form or mixed with red iron oxide (IO) pigment or lampblack (LB) (a carbon-based pigment historically obtained from the soot of oil lamps [31]). The mixture with the pigment was intended to reproduce a simplified version of the patinas that were applied in the past on the surface of the artefacts for aesthetic and/or protective functions [32]. The material layers were spread on glass or on metallic support (bronze (B)) in order to evaluate the influence of the substrate on fluorescence intensity, FL lifetime, and Raman spectra. The complete list of samples with their description can be found in Table 1.

Table 1. List of the analyzed samples with mean τ-phase and main Raman peaks.

Samples Description	Acronym	Mean τ-phase [ns] with (St. Dev.)	Principal Raman Signals [cm^{-1}]
Linseed oil	LO	2.44 (0.10)	727w, 866m, 972w, 1024w, 1078m, 1268ms, 1302ms, 1444s, 1658vs, 2727w, 2885m, 2932w, 3017w
Mastic	M	2.26 (0.10)	468w, 533w, 596m, 722m, 937m, 1200m, 1271w, 1315w, 1441ms, 1461sh, 1653ms, 1698sh, 2884sh, 2926m
Beeswax	BW	2.11 (0.10)	889w, 1063s, 1131s, 1172w, 1296s, 1419m, 1441s, 1464m, 2726w, 2850m, 2929sh
Iron oxide	IO	3.42 (0.10)	146w, 225s, 293vs, 410s, 497m, 611ms, 659br, 1317br
Lampblack	LB	3.28 (0.12)	1315s,br; 1591s,br
Beeswax + iron oxide on glass	BW + IO	2.90 (0.17)	225s *, 293vs *, 411s *, 498m *, 612ms *, 671br *, 1062m, 1131m, 1321br *, 1439m, 1464br, 2848w, 2883w
Mastic + iron oxide on glass	M + IO	2.65 (0.10)	147w *, 226s *, 293vs *, 412s *, 498m *, 612ms *, 662br *, 1320br *, 1448br, 1656w,br
Linseed oil + iron oxide on glass	LO + IO	2.36 (0.10)	227s *, 294vs *, 413s *, 495m *, 611m *, 866m,br, 1085m, 1303ms, 1441ms, 1662br, 1733br
Beeswax + lampblack on glass	BW + LB	2.97 (0.16)	1315s,br *; 1597s,br *
Mastic + lampblack on glass	M + LB	2.52 (0.10)	1314s,br *; 1445br, 1588s,br *, 2880br,sh, 2935br
Linseed oil + lampblack on glass	LO + LB	2.34 (0.10)	872br, 1087w, 1313s *, 1441s, 1596s *, 1732sh, 1856m, 2910m, 2936m
Linseed oil on bronze	LO(b)	2.26 (0.10)	1064w, 1080w, 1305m, 1439ms, 1654br, 1723br
Oleoresin (Linseed oil + mastic on bronze)	OR(b)	1.43 (0.10)	1063w, 1085w,1308m, 1444m, 1647br, 2863br, 2934br
Linseed oil + mastic + beeswax + iron oxide on bronze	LO + M + BW + IO(b)	1.65 (0.12)	227s *, 293s *, 413m *, 465w, 612m,br *, 10632, 1134w, 1175w, 1296m, 1442s, 1461sh, 1653w,br, 2852m, 2883m, 2938br

s—strong peaks, m—medium, ms—medium strong, v—very, w—weak, sh—shoulder, br—broad; * only for samples containing more than one component: Raman peaks attributable to a pigment

2.2. Fluorescence Lifetime Setup

Detailed descriptions of the prototype used for FL measurements are reported in [28] and [33]. The excitation source is a picosecond pulsed laser diode emitting at 375 nm (BDL-SMN-375, Becker & Hickl GmbH, Berlin, Germany) with a repetition rate of 20 MHz. Two 200 µm fibers deliver the excitation light and the aiming beam (λ = 660 nm, LED, M660FP1, Thorlabs) to the sample. The fiber bundle is handheld, and the tip is moved freely over the specimen. The collection of the fluorescence emitted from the sample is selected by an emission filter (FF01-510/84-25, Semrock, Rochester, New York, NY, USA) to the band 510 ± 42 nm. A third 200 µm fiber carries the signal to the detector (HPM-100-40, Becker & Hickl GmbH), which is connected to a TCSPC acquisition card (SPC-730, Becker & Hickl GmbH). For all measurements, the average power on the sample surface was kept below 10 µW.

Real-time fluorescence lifetime maps are acquired from single-point measurements at a macroscopic scale and, remarkably, under bright illumination. To allow the visual control of the examined area during measurements, the system is equipped with a white LED that provides periodic illumination of the field of view (FOV). The LED is turned on and off asynchronously with respect to the periodic detection of the fluorescence signal, thus overcoming the limitation related to the sensitivity of TCSPC to background light. The LED intensity was kept between 100 and 200 LUX, as measured at the sample plane, located 30 cm from the source. In addition, the 660 nm LED source was superimposed on the excitation beam to provide a visual reference for measurements. The sample was imaged in white light by a color CCD camera with an image resolution of 640 × 480 pixels so that the lifetime value obtained via phasor analysis for each acquisition point could be superimposed on the sample's surface. This enables the spatial resolution of the FL from single-point measurements, along with direct correlation with the spatial information provided by the raw white-light image.

Phasor Analysis

Fluorescence intensity decay measured on the samples' surfaces was analyzed using the phasor method; a comprehensive description of this approach can be found elsewhere [34]. In brief, assuming an infinitely short excitation pulse (δ-function) and an intrinsic fluoresce decay of N ($N \geq 1$), fluorescent species with distinct fluorescence lifetimes can be modeled by Equation (1):

$$I(t) = I(0) \sum_{i=0}^{N} \alpha_i e^{\frac{-t}{\tau_i}} \quad (1)$$

where $I(0)$ is the number of the instantly emitted photons at time zero; the coefficient α_i, called the pre-exponential factor, is the amplitude; and τ_i is the fluorescence decay time of the i-th component of the mixture.

The phasor analysis employs the Fourier transformation of the fluorescence intensity decay to produce real and imaginary components $\boldsymbol{g}$ and $\boldsymbol{s}$, respectively, which are calculated as follows:

$$g(\omega) = \int_0^T I(t) \cdot \cos(\omega t) dt / \int_0^T I(t) dt \quad (2)$$

$$s(\omega) = \int_0^T I(t) \cdot sen(\omega t) dt / \int_0^T I(t) dt \quad (3)$$

where $I(t)$ is the fluorescence intensity at a given timepoint t within the acquisition period T, and ω is the laser's angular frequency $\omega = 2\pi f$ (where f is the laser repetition rate). From the polar coordinates g and s, phase (τ-phase) lifetime can be calculated for each decay curve, as shown in Equation (4):

$$\tau_{phase} = \frac{1}{\omega} \frac{s}{g} \quad (4)$$

Each fluorescence decay is acquired from a group of pixels to generate FL maps. Fluorescence decay values can be plotted as a single point (phasor) in the phasor plot. For a single-lifetime species (N = 1), the FL can be directly determined by the coordinate values of the phasor. The relationship between the two coordinates of a phasor representing a single-lifetime species can be drawn as a semicircle curve (Equation (5)), centering at (g = 0.5; s = 0), with a radius of 0.5 in the phasor plot, called the universal semicircle or the universal trajectory.

$$(g - 0.5)^2 + s^2 = 0.25 \quad (5)$$

For multiple-lifetime species ($N > 1$), the phasor (g, s) is a linear combination of multiple phasors, each (g_i, s_i) representing an individual species. FL data can be analyzed and interpreted considering the following [34]: First, the universal semicircle is a lifetime ruler for single-lifetime species, and indicates relative changes in lifetime for complex species; the lifetimes increase from right to left—i.e., lifetimes near zero at (g = 1; s = 0), and infinite lifetimes at (g = 0; s = 0). Given the same single-lifetime value, the phasor shifts to the left along the semicircle for a lower modulation frequency ω, which results in an increase in the s/g ratio; this makes the phasor plot a very flexible tool to highlight the differences among the lifetime values. Moreover, a phasor plot centering at a point on the semicircle indicates a single-lifetime species, whereas a compound of a multiple-lifetime species falls inside the semicircle, with the phasor of a complex species being a linear combination of the individual phasors of single-lifetime species. Finally, the phasor of each fluorescent component contributing to the measured lifetime always falls inside the semicircle. Therefore, phasors located outside the semicircle should not be considered, as they result from signals that are strongly affected by perturbation from noise.

2.3. Raman Spectroscopy

Raman spectra were obtained with a Renishaw inVia Raman confocal microscope coupled with a Leica DM2700 optical microscope and a solid-state excitation source emitting at 785 nm. Measurements were performed in an extended spectral range of 100–3200 cm^{-1}, using a 1200 L/mm grating and a thermoelectrically cooled CCD detector (spectral range 400–1060 nm) with a spectral resolution of 1 cm^{-1} per CCD pixel (functional resolution of 3 cm^{-1}). The laser power on the material samples varied from 1 to 3.7 mW, depending on the material, with 10–20 s integration times and 20 accumulations. Data were collected with a 50× magnification objective (numerical aperture (NA) 0.75; theoretical spot size 0.6 μm) and processed with TWire5.2–5.5 and OriginPro software.

3. Results

Before the phasor lifetime analysis, fluorescence spectra of the individual materials were acquired using the same excitation wavelength used for FL measurements. The fluorescence bands of all spectra (Figure 1a) fell in the spectral range 450–650 nm, thus ensuring the suitability of the detection filter (510 ± 42 nm; light blue rectangle in Figure 1a) used to collect the FL signal. The shape and the central wavelength (≈525–540 nm) of the emission bands are in accordance with what can be found in the literature for these materials [5,35]. Raman analysis of the pure materials (Figure 1b,c) confirms the chemical composition of the probed materials, revealing the main peaks associated with them (see Table 1).

The binding materials belonged to three different groups: drying oil (linseed oil), natural wax (beeswax), and triterpenoid resin (mastic). In the Raman range analyzed, the spectra showed a background that varied according to the material. For mastic resin and beeswax, a stronger background competing with the characteristic Raman signals was observed. In the linseed oil, the background was lower and, therefore, the peaks were better resolved. The most intense peak in linseed oil (dried for 48 h, at room conditions) was at 1658 cm^{-1}, associated with the stretching vibration of a cis dialkyl C=C double bond in linoleic acid [36,37]. As to the mastic resin, the main Raman signals were revealed at 1441 cm^{-1}—with a shoulder at 1461 cm^{-1}—and 1652 cm^{-1}, corresponding to $\delta(CH_2)$,

$\nu(CH_2)$, and $\nu(C{=}C)$, respectively [38–41]. No bands associated with C=C vibrations were detected in the Raman spectrum of beeswax. The characteristic Raman bands at 1131 ν_{as}(C-C), 1172 ν(C-C), and 1419 $\delta(CH_3)$ [36,41] allowed the differentiation of beeswax from the other two binding materials.

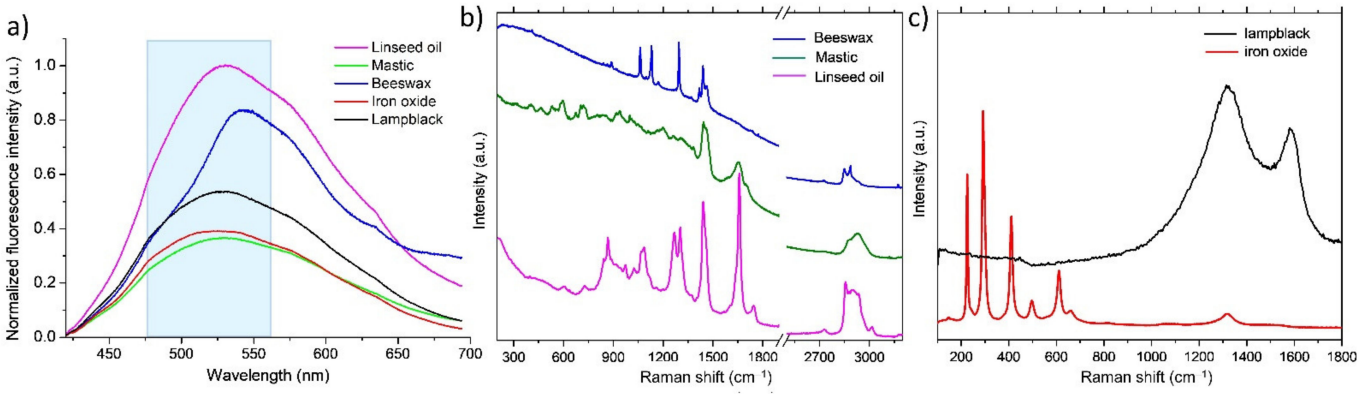

Figure 1. Fluorescence emission (**a**) and Raman (**b**,**c**) spectra of the analyzed materials.

Regarding the pigments, the Raman spectrum of the red pigment clearly shows the characteristic peaks of iron oxide at 225 cm^{-1}, 293 cm^{-1}, 410 cm^{-1}, 497 cm^{-1}, 611 cm^{-1}, 1317 cm^{-1}, assigned to ν_s(Fe-O), δ_s(Fe-O), and ν_{as}(Fe-OH) [42,43]. An additional peak at 659 cm^{-1} may belong to iron impurity in the form of magnetite, or to a disorder band in the crystalline structure of hematite, caused by exposure to a high temperature during burning [44,45]. On the other hand, the lampblack pigment is characterized by the two broad bands of amorphous carbon—at 1315 cm^{-1} and 1591 cm^{-1}—assigned to the D- and G-bands of CC, respectively [46,47].

FL measurements were performed on each sample using both single-point and imaging modes. Data were processed using the phasor method and, for all measurements, the τ-phase was calculated as an average over 3000 acquisition points with 20 ms integration time each in the imaging mode, and 20 points with 15 s integration time for each decay in the single-point mode. The uncertainty for each τ-phase value (reported in brackets in Table 1) is given by the maximum value between the standard deviation of the mean and the HWHM of the instrument response function (IRF) of 0.1 ns, measured as instrumental response to a laser pulse. Comparison of data provided by the two acquisition modalities showed that for most samples the imaging mode provides a more dispersed distribution of values than the single-point acquisition over the same region. A representative example is the linseed oil (LO) sample shown in Figure 2. The FL map (Figure 2b) is described by the color-scale distribution of g and s values in the phasor plot (Figure 2d), reported together with the values obtained via the single-point measurements (black circles in the diagram). The color scale of the density map corresponds to the number of decays with the same g and s values. As seen from the phasor plot, mean g and s values obtained with the imaging mode (g = 0.78 and s = 0.28) differed slightly from the respective values measured with the single-point approach (g = 0.82 and s = 0.29). The main moments characterizing the painting distribution for g and s coordinates—namely, variance, skewness, and kurtosis—are also reported in Figure 2d. The difference between the mean τ-phases derived from the imaging (2.89 $\pm$ 0.1 ns) and the single-point (2.44 $\pm$ 0.1 ns) modes is attributed to the reduced SNR of the imaging mode—caused by a shorter integration time—as well as to the fluctuation of the SNR introduced by the reduced distance stability between the sample and the probe, which is hand-held by the operator during the imaging acquisition. Such error becomes less significant when mapping a specimen composed of materials with very different fluorescence lifetimes (for example, the original and retouched areas of a painting). However, in this study, we chose to consider only point data, so as to provide a more precise characterization of the analyzed materials.

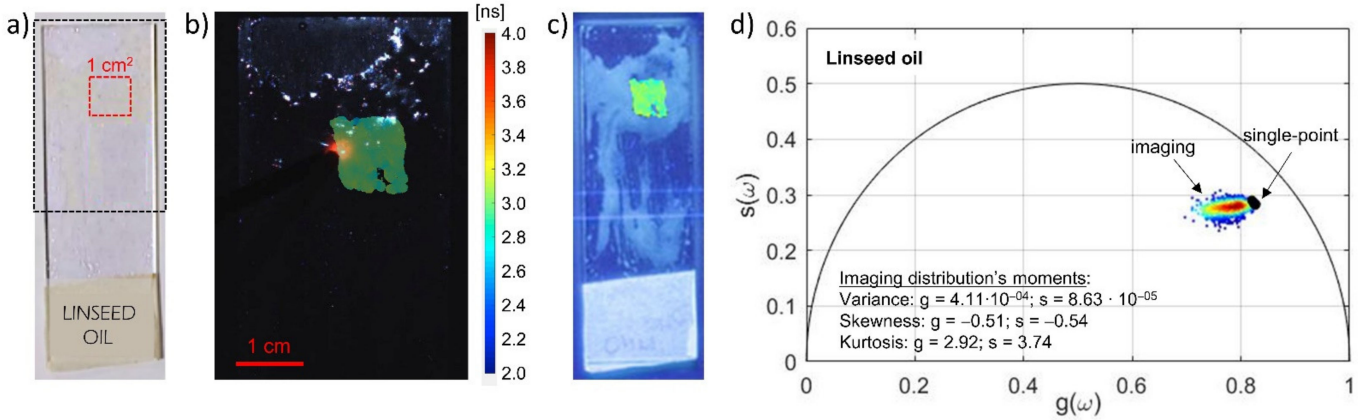

Figure 2. Imaging and single-point FL analysis of an LO sample. (**a**) Bright-field image of the sample, i.e., linseed oil spread on a microscope slide (the red dashed square indicates the region where measurements were acquired, while the black dashed rectangle shows the area magnified in (**b**), as seen by the CCD camera of the FL instrument working in imaging mode. (**b**) Detail of the sample showing the fluorescence lifetime map in color-coded scale obtained in imaging mode (color bar corresponding to the τ-phase values); the red spot is from the aiming beam. (**c**) The same lifetime map superimposed on the linseed oil sample, illuminated with a low-pressure mercury lamp. (**d**) Phasor diagram showing the distribution of phasors calculated from the imaging and the single-point modes on the same area.

The results of the lifetime phasor analysis of the linseed oil, mastic, and beeswax samples are reported in Figure 3. The τ-phase values of the three materials derived from the phasor plot are clearly distinguishable, resulting in 2.44 $\pm$ 0.1 ns, 2.26 $\pm$ 0.1 ns, and 2.11 $\pm$ 0.1 ns, respectively.

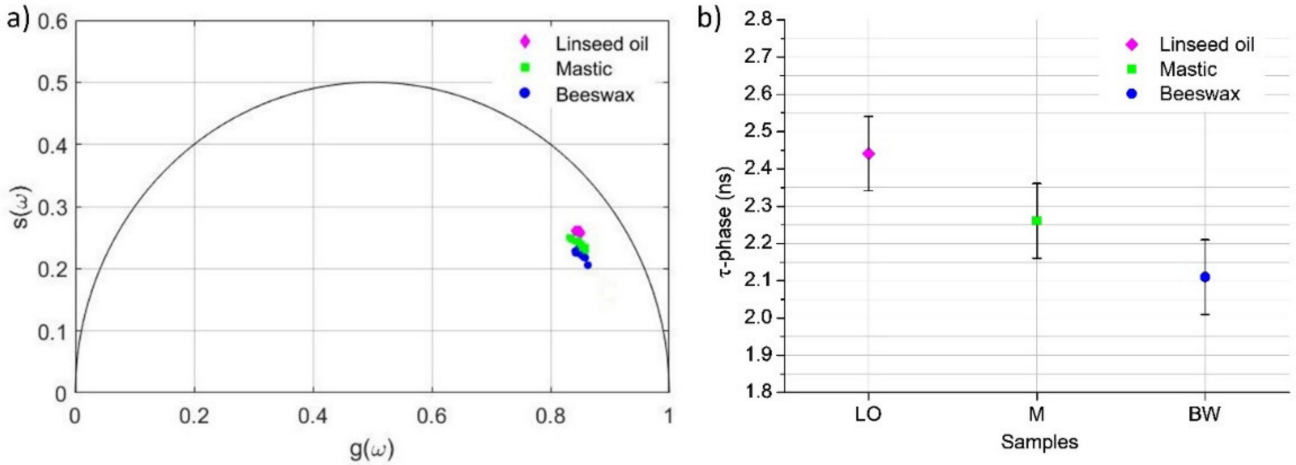

Figure 3. Results of the lifetime phasor analysis of LO, M, and BW samples: phasor plot (**a**) and plot of the mean τ-phase values (**b**), with corresponding standard deviations indicated by the error bars.

Figure 4a,c show the comparison of the τ-phases of the three binding materials mixed in comparable quantities with the red and the black pigments. The fluorescence lifetimes of iron oxide (IO) and lampblack (LB)—3.4 ns and 3.3 ns, respectively—are longer than those of the mixtures. In other words, the presence of the pigment in the binder results in an increase in the τ-phase of the pure binder—particularly for beeswax, which increases from 2.1 ns to ~3 ns in both the pigment mixtures. An increase in τ-phase, albeit less significant, is also observed in the mastic-based mixtures (M + IO and M + BW): the fluorescence lifetime of the pure resin (2.3 ns) becomes 2.6 ns with the addition of OI and 2.5 ns with LB. In contrast, the change in τ-phase is negligible for linseed oil, resulting in ~2.4 ns in

both the pure form and in the mixtures with the pigments. This difference in τ-phases is consistent with the Raman results of the mixed samples (Figure 4b,d), especially those based on linseed oil as compared to the other mixtures. The characteristic peaks of the oil compete in intensity with those of the pigment, confirming its lower influence on the overall Raman signal.

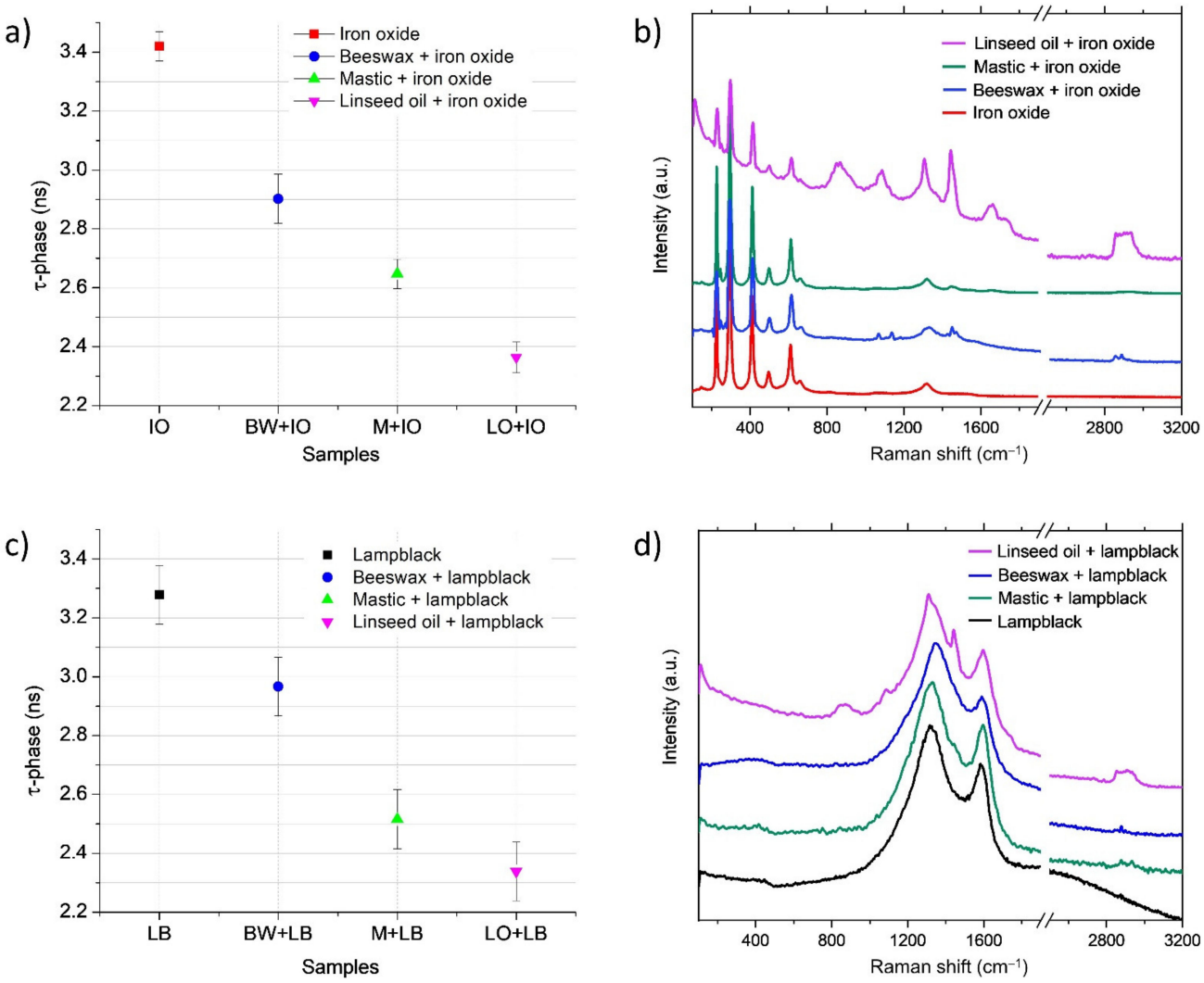

Figure 4. FL (**a**,**c**) and Raman (**b**,**d**) results for pigmented mixtures of LO, BW, and M.

Finally, we show the results of the combined FL–Raman analysis of the mixtures laid on bronze supports (Figure 5). Here, the advantage of integrating data from two complementary techniques is particularly evident. As noted above, in the case of linseed oil, the FL is very similar for both pigmented samples (LO + IO and LO + LB), making it difficult to recognize when the binder is in a pure form or mixed with the pigment—information that is easily identified via Raman spectroscopy. Furthermore, the influence of the metal substrate in LO(b) and OR(b) samples, as well as the co-presence of different fluorophore species in the OR(b) and LO + M + BW + IO(b) mixtures, makes it difficult to distinguish between one sample and another based on FL analysis alone (Figure 5a). These uncertainties are clarified by the Raman analysis (Figure 5b), showing more distinctly the contribution of individual components in the mixtures. In particular, both iron oxide and lampblack pigments are clearly identified in the Raman spectra of the mixtures LO + IO and LO + LB. The signal of LO is clearly revealed in its mixture with iron oxide pigment, while some of LO's relevant peaks are not detectable in its mixture with lampblack, due to

the overlap with the very strong bands of amorphous carbon (see Table 1 for the full list of detected Raman shift bands). I n the complex sample LO + M + BW + IO(b) containing a mixture of four components, Raman analysis contributes with identification of the inorganic pigment and a mixture of organic compounds. The peaks at 1134 cm^{-1} ν_{as}(C-C) and 1175 cm^{-1} ν(C-C) are attributable to beeswax, applied as the final layer; a shoulder at around 1460 cm^{-1} can be attributed to the presence of both beeswax and mastic, while a broad Raman signal around 1653 cm^{-1} ν(C=C) indicates the presence of linseed oil and mastic resin. The contribution of all the three components results in an intense peak of $\delta(CH_2)$ around 1442 cm^{-1}, and in the region of ν(C-H) vibrations (2850–2930 cm^{-1}).

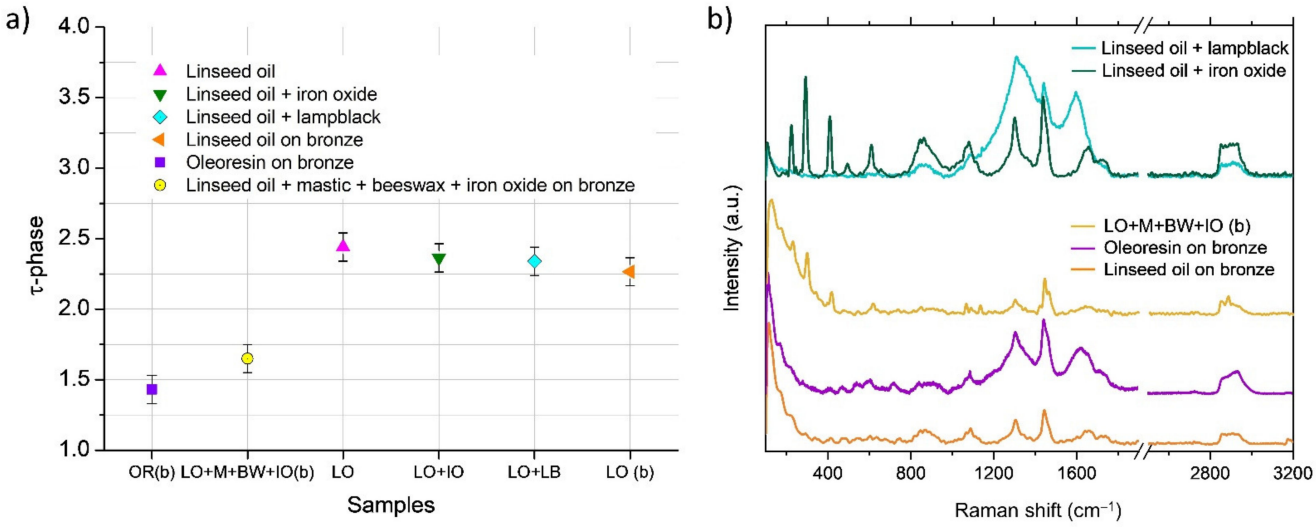

Figure 5. FL (**a**) and Raman (**b**) results for pigmented and non-pigmented mixtures laid on glass and metal substrates. Raman spectra are plotted after baseline subtraction (default function in TWiRE software).

4. Discussion

In this work, we investigated the effectiveness of the combination of time-resolved fluorescence and micro-Raman spectroscopy, taking the advantages of the different sensitivity of the two methods. Raman spectroscopy produces a spectral fingerprint that enables molecular characterization of the sample, but at the cost of relatively time-consuming measurements that are often limited by the inherent weakness of the Raman scattering phenomenon, which can be hampered by other competitive processes such as fluorescence. Implementation of the method to the fiber-based imaging mode is not straightforward, although the possibility of combining Raman–FL in a fiber probe for imaging has already been demonstrated [33]. On the other hand, the analysis of UV-induced fluorescence allows for a limited chemical specificity, especially when organic compounds are considered—such as binders and varnishes, which are composed of a variety of fluorophores that give rise to a broadband signal. Furthermore, FL phasor analysis has proven effective in discriminating different binders in real time with an easy-to-use fiber-based imaging modality. Hence, the combined use of the two techniques can provide both molecular fingerprinting and fast analysis by targeting both components of pigment–binder mixtures.

In pigmented mixtures, the influence of the pigments on the overall fluorescence signal is widely documented in the literature, and may depend on a number of competing factors, including optical scattering and absorption of fluorescence or luminescence emissions from the pigment, as well as chemical interactions (e.g., quenching) between the binder and the pigment [14,15,17]. The change in FL observed in this study shows a possible further correlation with the viscosity of the binder in which the pigment is dispersed. In the cases reported here, the fluorescence lifetime of the pigments seems to have been strongly affected by the high-viscosity medium—beeswax—while it remained almost unchanged

when mixed with linseed oil, which is characterized by a lower viscosity. It is known that the non-radiative decay of the excited state of a fluorophore is affected by the medium viscosity, which is one of the main parameters determining the diffusion of fluorescent species [48]. In low-viscosity media, the non-radiative decay via intramolecular charge transfer from the excited fluorophore to absorbing molecules in the surrounding environment is greater than in high-viscosity media, resulting in a decrease in the fluorescence lifetime [49]. Further measurements will allow for verification of this hypothesis. For now, the preliminary results presented in this work demonstrate that FL phasor analysis allows for discrimination between materials, and reveals very subtle differences in the decay times of pure or mixed substances.

The observed influence on the fluorescence lifetime by the bronze substrate is likely related to the presence of copper in the metal alloy. Indeed, copper(II) ions are well-known quenchers of fluorescence, not only producing evident changes in the fluorescence spectra of protein-based binding media [19], but also significantly reducing the fluorescence lifetime via a Förster resonance energy transfer (FRET) mechanism [50]. As with pigments dispersed in the binder, for mixtures laid on a bronze substrate, the reduction in lifetime can be also related to the concomitant release of non-radiative energy to the molecular environment.

5. Conclusions

This study demonstrates that the sensitivity of the FL of the emitting species to the surrounding molecular environment can be exploited to obtain specific information about organic binders in pure form, as a mixture with pigments, or laid on metal substrates. The compact size and portability of the proposed FL system, as well as the visual control of the analyzed area during the acquisition of a background-free fluorescence signal, make the technique particularly well suited for in situ measurements of a variety of CH objects. The integration of FL data with Raman spectroscopy allows us to overcome uncertainties due to very subtle differences between the measured τ-phases, demonstrating that the combination of the two techniques offers a powerful multi-analytical approach for the recognition and characterization of the art materials examined in this work. Therefore, a system combining the two techniques could be of great interest in heritage science. In view of FL mapping of artworks, further analyses in imaging mode on a wider range of art materials are planned in order to compare the results more thoroughly with respect to the single-point acquisition mode. Further analysis is also required in order to gain a deeper understanding of the mechanisms that influence the τ-phase of pigments dispersed in media with different viscosity, and in mixtures spread on copper-based metal substrates. Finally, investigations of aged samples are planned in order to test the applicability of the proposed method for the monitoring of degradation processes in artistic materials.

Author Contributions: Conceptualization, R.C. and R.F.; methodology, R.F., R.C., J.S., and A.D.F.; software, J.L.L.; validation, J.S.; formal analysis, S.M., D.Q.B., and A.C.; investigation, S.M., D.Q.B., and A.C.; data curation, S.M., D.Q.B., A.C., R.F., and A.D.F.; writing—original draft preparation, A.D.F.; writing—review and editing, A.D.F., S.M., D.Q.B., A.C., J.S., R.C., and R.F.; supervision, J.S., R.C., and R.F.; funding acquisition, R.F., J.S., and R.C. All authors have read and agreed to the published version of the manuscript.

Funding: This research was funded by Regione Toscana (POR FSE 2014–2020, "Giovanisì", Intervention Program "CNR4C", CUP B15J19001040004).

Institutional Review Board Statement: Not applicable.

Acknowledgments: Monica Galeotti from Opificio delle Pietre Dure is gratefully acknowledged for helping in the preparation of the samples, as well as for very fruitful discussions.

Conflicts of Interest: The authors declare no conflict of interest.

References

1. Lakowicz, J.R. *Principles of Fluorescence Spectroscopy*, 3rd ed.; Springer: London, UK, 2006. [CrossRef]
2. Hansell, P. Ultraviolet and Fluorescence Recording. In *Photography for the Scientist*; Engel, C., Ed.; Academic Press: London, UK; New York, NY, USA, 1968; pp. 363–382.
3. Mairinger, F. UV-, IR- and x-ray Imaging. In *Non-Destructive Microanalysis of Cultural Heritage Materials, Comprehensive Analytical Chemistry*; Janssens, K., Van Grieken, R., Eds.; Elsevier: Amsterdam, The Netherlands, 2004; Volume 42, pp. 15–66.
4. Comelli, D.; Valentini, G.; Cubeddu, R.; Toniolo, L. Fluorescence lifetime imaging for the analysis of works of art: Application to fresco paintings and marble sculptures. *J. Neutron Res.* **2006**, *14*, 81–90. [CrossRef]
5. De la Rie, E.R. Fluorescence of Paint and Varnish Layers. Parts 1–3. *Stud. Conserv.* **1982**, *27*, 1–7, 65–69, 102–108. [CrossRef]
6. Ghirardello, M.; Valentini, G.; Toniolo, L.; Alberti, R.; Gironda, M.; Comelli, D. Photoluminescence imaging of modern paintings: There is plenty of information at the microsecond timescale. *Microchem. J.* **2020**, *154*, 104618. [CrossRef]
7. Anglos, D.; Georgiou, S.; Fotakis, C. Lasers in the analysis of cultural heritage materials. *J. Nano Res.* **2009**, *8*, 47–60. [CrossRef]
8. Romani, A.; Clementi, C.; Miliani, C.; Favaro, G. Fluorescence Spectroscopy: A Powerful Technique for the Noninvasive Characterization of Artwork. *Acc. Chem. Res.* **2010**, *43*, 837–846. [CrossRef]
9. Verri, G.; Saunders, D. Xenon Flash for Refectance and Luminescence (Multispectral) Imaging in Cultural Heritage Applications. *Br. Mus. Tech. Bull.* **2014**, *8*, 83–92.
10. Thoury, M.; Elias, M.; Frigerio, J.M.; Barthou, C. Nondestructive varnish identification by ultraviolet fluorescence spectroscopy. *Appl. Spectrosc.* **2007**, *61*, 1275–1282. [CrossRef]
11. Nevin, A.; Comelli, D.; Valentini, G.; Cubeddu, R. Total Synchronous Fluorescence Spectroscopy Combined with Multivariate Analysis: Method for the Classification of Selected Resins, Oils, and Protein-Based Media Used in Paintings. *Anal. Chem.* **2009**, *81*, 1784–1791. [CrossRef]
12. Nevin, A.; Spoto, G.; Anglos, D. Laser spectroscopies for elemental and molecular analysis in art and archaeology. *Appl. Phys. A* **2012**, *106*, 339–361. [CrossRef]
13. Striova, J.; Dal Fovo, A.; Fontana, R. Reflectance imaging spectroscopy in heritage science. *Riv. Nuovo Cim.* **2020**, *43*, 515–566. [CrossRef]
14. Clementi, C.; Miliani, C.; Verri, G.; Sotiropoulou, S.; Romani, A.; Brunetti, B.G.; Sgamellotti, A. Application of the Kubelka-Munk Correction for Self-Absorption of Fluorescence Emission in Carmine Lake Paint Layers. *Appl. Spectrosc.* **2009**, *63*, 1323–1330. [CrossRef] [PubMed]
15. Nevin, A.; Cesaratto, A.; Bellei, S.; D'Andrea, C.; Toniolo, L.; Valentini, G.; Comelli, D. Time-resolved photoluminescence spectroscopy and imaging: New approaches to the analysis of cultural heritage and its degradation. *Sensors* **2014**, *14*, 6338–6355. [CrossRef]
16. Elias, M.; Magnain, C.; Barthou, C.; Nevin, A.; Comelli, D.; Valentini, G. UV-fluorescence spectroscopy for identification of varnishes in works of art: Influence of the underlayer on the emission spectrum. In *O3A: Optics for Arts, Architecture, and Archaeology II*; International Society for Optics and Photonics: Bellingham, WA, USA, 2009; Volume 7391, p. 739104.
17. Verri, G.; Clementi, C.; Comelli, D.; Cather, S.; Piqueé, F. Correction of ultraviolet-induced fluorescence spectra for the examination of polychromy. *Appl. Spectrosc.* **2008**, *62*, 1295–1302. [CrossRef] [PubMed]
18. Nevin, A.; Comelli, D.; Valentini, G.; Anglos, D.; Burnstock, A.; Cather, S.; Cubeddu, R. Time-resolved fluorescence spectroscopy and imaging of proteinaceous binders used in paintings. *Anal. Bioanal. Chem.* **2007**, *388*, 1897–1905. [CrossRef]
19. Nevin, A.; Anglos, D. Assisted interpretation of laser-induced fluorescence spectra of egg-based binding media using total emission fluorescence spectroscopy. *Laser Chem.* **2006**, *2006*, 82823. [CrossRef]
20. Comelli, D.; Nevin, A.B.; Verri, G.; Valentini, G.; Cubeddu, R. Time-resolved fluorescence spectroscopy and fluorescence lifetime imaging for the analysis of organic materials in wall painting replicas. In *Organic Materials in Wall Paintings*; Project Report; Piqué, F., Verri, G., Eds.; Getty Conservation Institute: Los Angeles, CA, USA, 2015; pp. 83–96.
21. Comelli, D.; Nevin, A.; Valentini, G.; Osticioli, I.; Castellucci, E.M.; Toniolo, L.; Gulotta, D.; Cubeddu, R. Insights into Masolino's wall paintings in Castiglione Olona: Advanced reflectance and fluorescence imaging analysis. *J. Cult. Herit.* **2011**, *12*, 11–18. [CrossRef]
22. Artesani, A.; Ghirardello, M.; Mosca, S.; Nevin, A.; Valentini, G.; Comelli, D. Combined photoluminescence and Raman microscopy for the identification of modern pigments: Explanatory examples on cross-sections from Russian avant-garde paintings. *Herit. Sci.* **2019**, *7*, 17. [CrossRef]
23. Comelli, D.; Toja, F.; D'Andrea, C.; Toniolo, L.; Valentini, G.; Lazzari, M.; Nevin, A. Advanced non-invasive fluorescence spectroscopy and imaging for mapping photo-oxidative degradation in acrylonitrile–butadiene–styrene: A study of model samples and of an object from the 1960s. *Polym. Degrad. Stab.* **2014**, *107*, 356–365. [CrossRef]
24. Osticioli, I.; Mendes, N.F.C.; Nevin, A.; Zoppi, A.; Lofrumento, C.; Becucci, M.; Castellucci, E.M. A new compact instrument for Raman, laser-induced breakdown, and laser-induced fluorescence spectroscopy of works of art and their constituent materials. *Rev. Sci. Instrum.* **2009**, *80*, 076109. [CrossRef]
25. Martínez-Hernández, A.; Oujja, M.; Sanz, M.; Carrasco, E.; Detalle, V.; Castillejo, M. Analysis of heritage stones and model wall paintings by pulsed laser excitation of Raman, laser-induced fluorescence and laser-induced breakdown spectroscopy signals with a hybrid system. *J. Cult. Herit.* **2018**, *32*, 1–8. [CrossRef]

26. Accorsi, G.; Verri, G.; Bolognesi, M.; Armaroli, N.; Clementi, C.; Miliani, C.; Romani, A. The exceptional near-infrared luminescence properties of cuprorivaite (Egyptian blue). *Chem. Commun.* **2009**, *23*, 3392–3394. [CrossRef] [PubMed]
27. Grazia, C.; Clementi, C.; Miliani, C.; Romani, A. Photophysical properties of alizarin and purpurin Al(III) complexes in solution and in solid state. *Photochem. Photobiol. Sci.* **2011**, *10*, 1249–1254. [CrossRef]
28. Lagarto, J.L.; Shcheslavskiy, V.; Pavone, F.S.; Cicchi, R. Real-time fiber-based fluorescence lifetime imaging with synchronous external illumination: A new path for clinical translation. *J. Biophotonics* **2020**, *13*, e201960119. [CrossRef]
29. Lagarto, J.L.; Villa, F.; Tisa, S.; Zappa, F.; Shcheslavskiy, V.; Pavone, F.S.; Cicchi, R. Real-time multispectral fluorescence lifetime imaging using Single Photon Avalanche Diode arrays. *Sci. Rep.* **2020**, *10*, 8116. [CrossRef]
30. Osete-Cortina, L.; Doménech-Carbó, M.T. Analytical characterization of diterpenoid resins present in pictorial varnishes using pyrolysis–gas chromatography–mass spectrometry with on line trimethylsilylation. *J. Chromatogr. A* **2005**, *1065*, 265–278. [CrossRef]
31. Lluveras-Tenorio, A.; Spepi, A.; Pieraccioni, M.; Legnaioli, S.; Lorenzetti, G.; Palleschi, V.; Vendrell, M.; Colombini, M.P.; Tinè, M.R.; Duce, C.; et al. A multi-analytical characterization of artists' carbon-based black pigments. *J. Therm. Anal. Calorim.* **2019**, *138*, 3287–3299. [CrossRef]
32. Matteini, M. *Le Patine: Genesi, Significato, Conservazione*; Nardini: Firenze, Italy, 2005; pp. 1–110.
33. Lagarto, J.L.; Shcheslavskiy, V.; Pavone, F.S.; Cicchi, R. Simultaneous fluorescence lifetime and Raman fiber-based mapping of tissues. *Opt. Lett.* **2020**, *45*, 2247–2250. [CrossRef]
34. Liao, S.-C.; Sun, Y.; Ulas, C. *FLIM Analysis Using the Phasor Plots*; ISS, Inc.: Champaign, IL, USA, 2014; Volume 61822.
35. Pelagotti, A.; Pezzati, L.; Bevilacqua, N.; Vascotto, V.; Reillon, V.; Daffara, C. A study of UV fluorescence emission of painting materials. In Proceedings of the 8th International Conference on Non-Destructive Investigations and Microanalysis for the Diagnostics and Conservation of the Cultural and Environmental Heritage (Art '05), Lecce, Italy, 15–19 May 2005; p. A97.
36. Vandenabeele, P.; Wehling, B.; Moens, L.; Edwards, H.; De Reu, M.; Van Hooydonk, G. Analysis with micro-Raman spectroscopy of natural organic binding media and varnishes used in art. *Anal. Chim. Acta* **2000**, *407*, 261–274. [CrossRef]
37. Schoenemann, A.; Edwards, H. Raman and FTIR microspectroscopic study of the alteration of Chinese tung oil and related drying oils during ageing. *Anal. Bioanal. Chem.* **2011**, *400*, 1173–1180. [CrossRef] [PubMed]
38. Osticioli, I.; Ciofini, D.; Mencaglia, A.A.; Siano, S. Automated characterization of varnishes photo-degradation using portable T-controlled Raman spectroscopy. *Spectrochim. Acta A* **2017**, *172*, 182–188. [CrossRef]
39. Nevin, A.; Comelli, D.; Osticioli, I.; Toniolo, L.; Valentini, G.; Cubeddu, R. Assessment of the ageing of triterpenoid paint varnishes using fluorescence, Raman and FTIR spectroscopy. *Anal. Bioanal. Chem.* **2009**, *395*, 2139–2149. [CrossRef] [PubMed]
40. Ciofini, D.; Striova, J.; Camaiti, M.; Siano, S. Photo-oxidative kinetics of solvent and oil-based terpenoid varnishes. *Polym. Degrad. Stab.* **2016**, *123*, 47–61. [CrossRef]
41. Edwards, H.G.; Farwell, D.W.; Daffner, L. Fourier-transform Raman spectroscopic study of natural waxes and resins. I. *Spectrochim. Acta Part A* **1996**, *52*, 1639–1648. [CrossRef]
42. Boucherit, N.; Hugot-Le Goff, A.; Joiret, S. Raman studies of corrosion films frown on Fe and Fe-6Mo in pitting conditions. *Corros. Sci.* **1991**, *32*, 497–507. [CrossRef]
43. Froment, F.; Tournié, A.; Colomban, P. Raman identification of natural red to yellow pigments: Ochre and iron-containing ores. *J. Raman Spectrosc.* **2008**, *39*, 560–568. [CrossRef]
44. Hanesh, M. Raman spectroscopy of iron oxides and (oxy)hydroxides at low laser power and possible applications in environmental magnetic studies. *Geophys. J. Int.* **2009**, *177*, 941–948. [CrossRef]
45. Kendrix, E.; Moscardi, G.; Mazzeo, R.; Baraldi, P.; Prati, S.; Joseph, E.; Capelli, S. Far infrared and Raman spectroscopy analysis of inorganic pigments. *J. Raman Spectrosc.* **2008**, *39*, 1104–1112. [CrossRef]
46. Coccato, A.; Jehlicka, J.; Moens, L.; Vandenabeele, P. Raman spectroscopy for the investigation of carbon-based black pigments. *J. Raman Spectrosc.* **2015**, *46*, 1003–1015. [CrossRef]
47. Tomasini, E.P.; Halac, E.B.; Reinoso, M.; Di Liscia, E.J.; Maier, M.S. Micro-Raman Spectroscopy of Carbon-based Black Pigments. *J. Raman Spectrosc.* **2012**, *43*, 1671–1675. [CrossRef]
48. Kuimova, M.K.; Yahioglu, G.; Levitt, J.A.; Suhling, K. Molecular rotor measures viscosity of live cells via fluorescence lifetime imaging. *J. Am. Chem. Soc.* **2008**, *130*, 6672–6673. [CrossRef] [PubMed]
49. Haidekker, M.A.; Theodorakis, E.A. Molecular rotors—Fluorescent biosensors for viscosity and flow. *Org. Biomol. Chem.* **2007**, *5*, 1669–1678. [CrossRef] [PubMed]
50. Hötzer, B.; Ivanov, R.; Altmeier, S.; Kappl, R.; Jung, G. Determination of copper(II) ion concentration by lifetime measurements of green fluorescent protein. *J. Fluoresc.* **2011**, *21*, 2143–2153. [CrossRef] [PubMed]